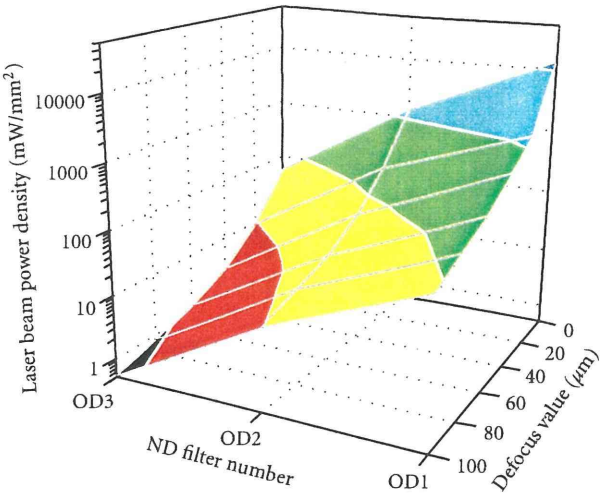

FIGURE 4: Power density of the Raman excitation laser beam measured as a function of ND filter number and the defocus value.

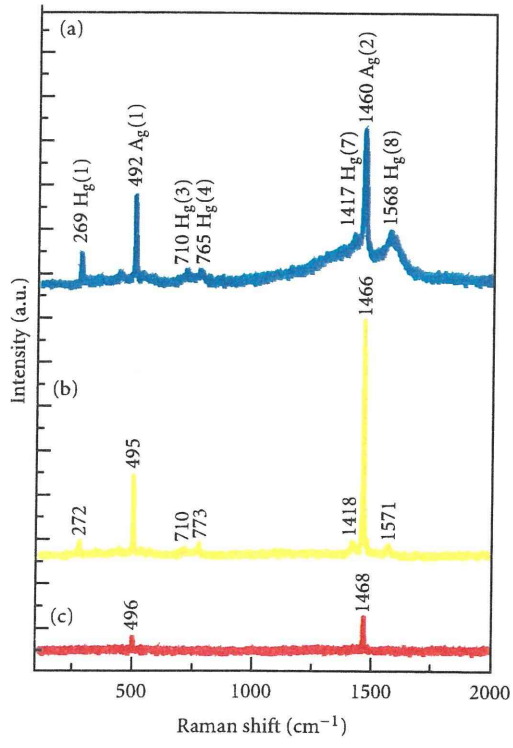

FIGURE 5: Raman spectra of C_{60}NWs. The power density of laser beam (D) is (a) 11800, (b) 1660, and (c) 71.5 mW/mm², respectively.

the red arrows for the high energy doses in Figures 6(c), 6(d), 6(e), and 6(f). These phenomena are supposed to be explained by the temperature rise of the C_{60}NWs exposed to the laser beams, since it is known that the photopolymerized C_{60} molecules decompose into their primary monomers and dimers by heating at temperatures higher than about 100°C [13].

The data points obtained using the highest power densities are indicated in each graph of Figure 6 by the black arrows for the exposure time of about 220 s. Figure 7 shows the relationship between the laser beam energy dose and the $A_g(2)$ peak position for the arrowed data points of Figure 6. The fitted curve of semilog plot is expressed as $y = -2.2x + 1467$, where x represents $\log_{10}$ (laser beam energy dose) and y represents the Raman shift of $A_g(2)$ peak. Using this experimental formula, the energy dose more than about 1520 J/mm² is found to be necessary for the photopolymerization of C_{60}NWs in air, when the laser light with a wavelength of 532 nm is used.

Since it is known that the photopolymerization of C_{60} progresses through the formation of four-membered rings between adjacent C_{60} molecules [11], it is considered that

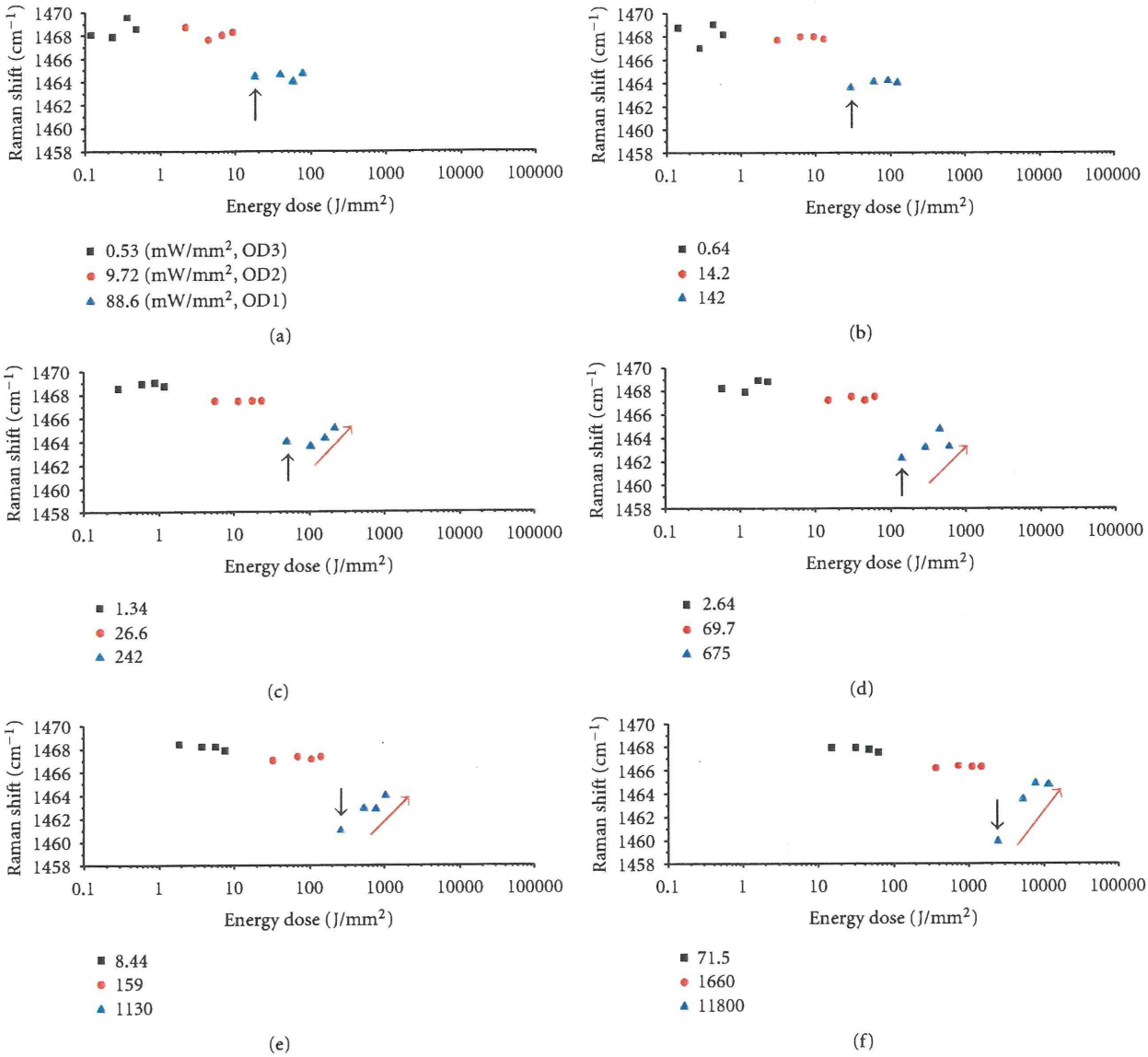

FIGURE 6: $A_g(2)$ peak positions of the Raman spectra of C_{60}NWs under various exposure conditions at the defocus values of (a) 100 μm, (b) 80 μm, (c) 60 μm, (d) 40 μm, (e) 20 μm, and (f) 0 μm (just focus), corresponding to (a) ~ (f) of Figure 3.

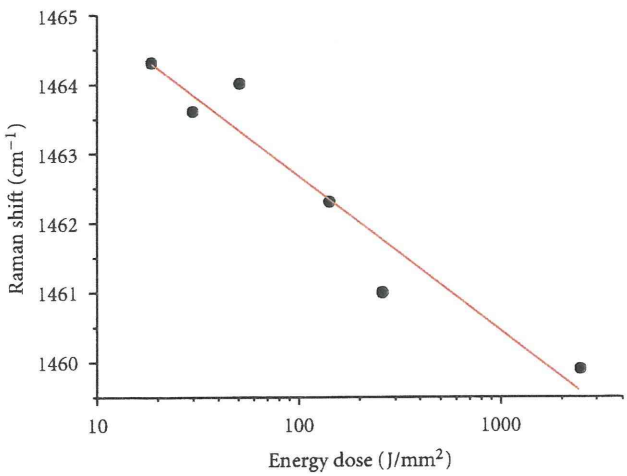

FIGURE 7: Relationship between the Raman shift of $A_g(2)$ peak and the energy dose of C_{60}NWs irradiated by the excitation laser beams.

C_{60} molecules are linearly polymerized by forming the four-membered rings along the growth axis of C_{60}NWs, as was shown in Figure 6 of [2].

In the gas chromatography-mass spectrometry (GC-MS) measurement of solvents contained in the C_{60}NWs that were prepared by use of toluene and IPA, the major residual solvent was toluene, and the content of IPA was very small compared with toluene [14]. Since the residual toluene of C_{60}NWs was measured to be about 0.2% after drying in an Ar atmosphere at 100°C for 30 min. [14], it is considered that the residual toluene of the vacuum-dried samples of C_{60}NWs in the present experiment is negligible and does not influence the Raman profiles.

4. Conclusions

The photopolymerization of C_{60}NWs was investigated by using the Raman laser beam of 532 nm wavelength at various

exposure conditions for the power density and the exposure time in air.

The $A_g(2)$ peak of C_{60}NWs shifted to the lower wavenumbers from that of the as-grown dried C_{60}NWs. However, the $A_g(2)$ peaks were found to move to the higher wavenumbers from the polymerized positions by the irradiation of laser beams for high energy doses at high-power densities, indicating the thermal dissociation of polymerized C_{60} molecules owing to the temperature rise.

An energy dose larger than about 1520 J/mm^2 was found to be necessary for the laser beam of 532 nm wavelength to obtain the photopolymerized C_{60}NWs.

Acknowledgment

Part of this research was supported by Health and Labour Sciences Research Grants (H21-Chemistry-Ippan-008) from the Ministry of Health, Labour, and Welfare of Japan.

References

[1] K. Miyazawa, "Synthesis and properties of fullerene nanowhiskers and fullerene nanotubes," *Journal of Nanoscience and Nanotechnology*, vol. 9, no. 1, pp. 41–50, 2009.

[2] K. Miyazawa, Y. Kuwasaki, A. Obayashi, and M. Kuwabara, "C_{60} nanowhiskers formed by the liquid-liquid interfacial precipitation method," *Journal of Materials Research*, vol. 17, no. 1, pp. 83–88, 2002.

[3] K. Ogawa, T. Kato, A. Ikegami et al., "Electrical properties of field-effect transistors based on C_{60} nanowhiskers," *Applied Physics Letters*, vol. 88, no. 11, Article ID 112109, 3 pages, 2006.

[4] P. R. Somani, S. P. Somani, and M. Umeno, "Toward organic thick film solar cells: three dimensional bulk heterojunction organic thick film solar cell using fullerene single crystal nanorods," *Applied Physics Letters*, vol. 91, no. 17, Article ID 173503, 3 pages, 2007.

[5] X. Zhang, Y. Qu, G. Piao, J. Zhao, and K. Jiao, "Reduced working electrode based on fullerene C_{60} nanotubes@DNA: characterization and application," *Materials Science and Engineering B*, vol. 175, no. 2, pp. 159–163, 2010.

[6] M. Nakaya, T. Nakayama, and M. Aono, "Fabrication and electron-beam-induced polymerization of C_{60} nanoribbon," *Thin Solid Films*, vol. 464-465, pp. 327–330, 2004.

[7] M. Tachibana, K. Kobayashi, T. Uchida, K. Kojima, M. Tanimura, and K. Miyazawa, "Photo-assisted growth and polymerization of C_{60} "nano"whiskers," *Chemical Physics Letters*, vol. 374, no. 3-4, pp. 279–285, 2003.

[8] K. Miyazawa, J. Minato, M. Fujino, and T. Suga, "Structural investigation of heat-treated fullerene nanotubes and nanowhiskers," *Diamond and Related Materials*, vol. 15, no. 4–8, pp. 1143–1146, 2006.

[9] K. Asaka, R. Kato, K. Miyazawa, and T. Kizuka, "Buckling of C_{60} whiskers," *Applied Physics Letters*, vol. 89, no. 7, Article ID 071912, 3 pages, 2006.

[10] D. Koide, S. Kato, E. Ikeda, N. Iwata, and H. Yamamoto, "Free electron laser-polymerization of C_{60} grown by liquid-liquid-interfacial precipitation method," *IEICE Transactions on Electronics*, vol. 94, no. 2, pp. 151–156, 2011.

[11] A. M. Rao, P. Zhou, K. A. Wang et al., "Photoinduced polymerization of solid C_{60} films," *Science*, vol. 259, no. 5097, pp. 955–957, 1993.

[12] E. Alvarez-Zauco, H. Sobral, E. V. Basiuk, J. M. Saniger-Blesa, and M. Villagrán-Muniz, "Polymerization of C_{60} fullerene thin films by UV pulsed laser irradiation," *Applied Surface Science*, vol. 248, no. 1–4, pp. 243–247, 2005.

[13] Y. Wang, J. M. Holden, X. X. Bi, and P. C. Eklund, "Thermal decomposition of polymeric C_{60}," *Chemical Physics Letters*, vol. 217, no. 4, pp. 413–417, 1994.

[14] M. Watanabe, K. Hotta, K. Miyazawa, and M. Tachibana, "GC-MS analysis of the solvents contained in C_{60} nanowhiskers," *Journal of Physics: Conference Series*, vol. 159, no. 1, Article ID 012010, 2009.

The Journal of Toxicological Sciences (J. Toxicol. Sci.)
Vol.37, No.2, 317-327, 2012

Original Article

Lack of promoting effect of titanium dioxide particles on chemically-induced skin carcinogenesis in rats and mice

Yoko Sagawa[1,2], Mitsuru Futakuchi[2], Jiegou Xu[2,3], Katsumi Fukamachi[2], Yuto Sakai[2,4], Yoshiaki Ikarashi[5], Tetsuji Nishimura[5], Masumi Suzui[2], Hiroyuki Tsuda[3] and Akimichi Morita[1]

[1]Department of Geriatric and Environmental Dermatology and [2]Department of Molecular Toxicology, Nagoya City University Graduate School of Medical Sciences, 1-Kawasumi, Mizuho-cho, Mizuho-ku, Nagoya 467-8601, Japan
[3]Nanotoxicology Project Laboratory, Nagoya City University and [4]Department of Drug Metabolism and Disposition, Nagoya City University Graduate School of Pharmaceutical Sciences, 3-1 Tanabedohri, Mizuho-ku, Nagoya 467-8603, Japan
[5]Division of Environmental Chemistry, National Institute of Health Sciences, 1-18-1 Kamiyoga, Setagaya-ku, Tokyo 158-8501, Japan

(Received December 5, 2011; Accepted December 27, 2011)

ABSTRACT — Nano-sized titanium dioxide particles (TiO_2) are widely used in cosmetics, sunscreens and food additives. We previously reported that topical application of non-coated rutile type TiO_2 did not exhibit a promoting effect on ultraviolet B-initiated skin carcinogenesis in rats, and that this was likely due to lack of penetration of TiO_2 into the epidermis. In the present study, we examined the promoting effect of silicone coated TiO_2 ($sTiO_2$) suspended in silicone oil and non-coated TiO_2 ($ncTiO_2$) suspended in Pentalan 408 on a two-stage skin chemical carcinogenesis model: $sTiO_2$ suspended in silicon oil forms smaller particles than $ncTiO_2$ suspended in Pentalan because of the smaller sizes of aggregates formed. The model used skin carcinogenesis-sensitive human c-Ha-ras proto-oncogene transgenic mice (rasH2) and rats (Hras128) and their wild-type counterparts and CD-1 mice to test the effects of topical application of TiO_2. Animals were initially treated with a single dose of 7,12-dimethylbenz[a]anthracene (DMBA) and then with 0, 10, or 20 mg $sTiO_2$ (mice) or 0, 50, or 100 mg $ncTiO_2$ (rats). The incidence and multiplicity of skin tumors (squamous cell papilloma and carcinoma) did not increase over DMBA alone controls in skin carcinogenesis-sensitive mice or rats or wild-type animals. Analysis of rat skin indicated that $sTiO_2$ and $ncTiO_2$ did not penetrate though either healthy or damaged skin. Furthermore $sTiO_2$ did not penetrate an *in vitro* human epidermis model. Our results indicate that treatment with $sTiO_2$ or $ncTiO_2$ did not promote skin carcinogenesis in mice or rats, probably due to lack of penetration through the epidermis.

Key words: Nano-size TiO_2, Skin carcinogenesis, Hras, Rat, Mouse

INTRODUCTION

Nano-sized titanium dioxide (TiO_2) particles are used in sunscreen formulations to protect against skin lesions caused by exposure to UV light (Gelis *et al.*, 2003; Rouabhia *et al.*, 2002; Suzuki, 1987). Nano and larger scale titanium dioxide particles are known to be carcinogenic to the rat lung (Baan *et al.*, 2006; Baan, 2007). Recently, we demonstrated a promoting effect on rat lung carcinogenesis by nano-size TiO_2 particles administered by a novel intrapulmonary spraying method (Xu *et al.*, 2010). The mechanism of promotion of lung carcinogenesis involved the induction of MIP1α protein expression by $ncTiO_2$-laden alveolar macrophages (Xu *et al.*, 2010).

We also examined the carcinogenic effect of TiO_2 (mean manufacturer's particulate diameter of 20 nm) on the skin in a UVB-initiated two-stage rat carcinogenesis model and found that topical application of TiO_2 did not promote skin carcinogenesis in this model. This result is probably due to the inability of TiO_2 to penetrate through

Correspondence: Akimichi Morita (E-mail: amorita@med.nagoya-cu.ac.jp)

the epidermis and reach the underlying tissue (Xu *et al.*, 2011). This speculation is consistent with a report by Newman *et al.* (2009) demonstrating an absence of penetration of TiO_2 through the epidermis and hair follicles (Newman *et al.*, 2009). On the other hand, Wu *et al.* (2009) reported that TiO_2 (4 nm and 60 nm length) could penetrate through the stratum corneum (SC) and become located in the deep layer of the epidermis after being topically applied to pig ear for 30 days (Wu *et al.*, 2009). These inconsistent observations may be due to differences in particle size and the animals used.

The skin is histologically composed of the SC, epidermis, dermis and the subcutaneous tissue. The SC is the rate-limiting barrier against exposure to various exogenous chemical and physical agents (Schaefer *et al.*, 2003). For solid materials, including nano-sized particles, to cause inflammatory lesions, they need to penetrate the SC to interact with macrophages and other inflammatory leucocytes. Long-term activation of inflammatory leukocytes has the potential to cause skin carcinogenesis. Thus, the potential skin-carcinogenicity of TiO_2 is dependent on its size and ability to penetrate through the SC.

The surface of the TiO_2 used in cosmetics is usually coated with aluminum oxide or silicone oils to prevent aggregate formation and to enhance dispersal (Nohynek *et al.*, 2008). The particle size of TiO_2 suspended in silicone oils is known to be smaller than that of non-coated TiO_2 suspensions (Senzui *et al.*, 2010; also compare Fig. 1E with Fig. 1F). In our previous study, we showed that rutile type non-coated TiO_2 ($ncTiO_2$) did not penetrate the epidermal tissue and thus did not cause promotion of chemically-induced skin carcinogenesis. In the present study, we used rutile type TiO_2 coated with silicone ($sTiO_2$) suspended in silicon oil to minimize aggregation and improve the penetrating ability of the particles.

The ability of $sTiO_2$ suspended in silicone oil and $ncTiO_2$ suspended in Pentalan408 to promote skin carcinogenesis was examined using the 7,12-dimethylbenz[a] anthracene (DMBA)-initiated skin carcinogenesis model employing skin carcinogenesis-sensitive animals and their wild-type counterparts as the test animals. The rasH2 mouse carries a human c-Ha-ras proto-oncogene and is highly susceptible to chemically induced skin carcinogenesis (Muto *et al.*, 2006). The Hras128 rat also carries a human c-Ha-ras proto-oncogene and highly susceptible to chemically induced skin carcinogenesis (Park *et al.*, 2004).

In addition to the animal models, we also used an *in vitro* model to examine $sTiO_2$ particle penetration into skin. Unlike animal skin, the *in vitro* model does not have hair follicles, allowing direct examination of the ability of $sTiO_2$ particles to penetrate through a layer of human skin epidermal keratinocytes.

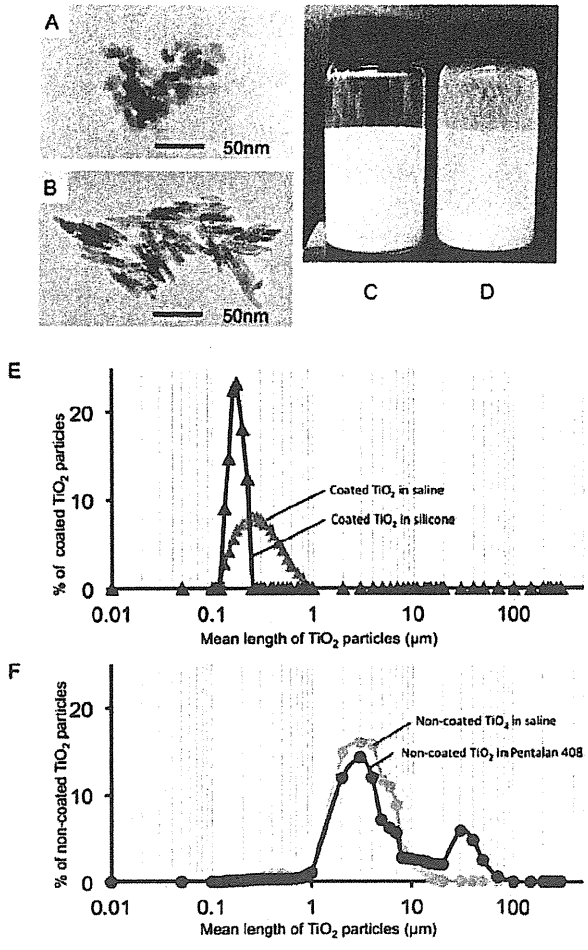

Fig. 1. Physicochemical features of $sTiO_2$ / $ncTiO_2$. $sTiO_2$ particles were round to oval in shape (A), and $ncTiO_2$ particles were club shaped (B). $sTiO_2$ particles remained evenly dispersed in silicone solution (C) while $ncTiO_2$ particles formed a white sediment at the bottom of the bottle 3 days after preparation (D). Size distribution of $sTiO_2$ suspended in saline (gray triangles) and in silicone (black triangles) (E). Size distribution of $ncTiO_2$ suspended in saline (gray circles) and in Pentalan 408 (black circles) (F). % of TiO_2 particles (Y axis) was calculated as the ratio of TiO_2 particles of a particular mean length/total particles examined.

Table 1. TiO_2 materials and animal strains used in this study

Coating status of TiO_2	Size	Concentrartion of TiO_2 (mg/ml)	Suspended in	Skin assay (Carcinogen) Strain (or *in vitro* system)
Coated (rutile type)	35 nm	50, 100	Silicone	Carcinogenesis (DMBA) rasH2 mouse, C57BL mouse
		100, 200	Silicone	Penetration LabCyte EPI-MODEL
Non-coated (rutile type)	20 nm	100, 200	Pentalan 408	Carcinogenesis (DMBA) Hras128 rat, Sprague-Dawley rat
		50, 100	Pentalan 408	Carcinogenesis (DMBA) CD1 mouse
		200	Pentalan 408	Penetration Sprague-Dawley rat

MATERIALS AND METHODS

Animals

Male rasH2 mice and Hras128 rats, known to be highly sensitive to chemically induced skin carcinogenesis (Muto *et al.*, 2006; Park *et al.*, 2004), and their wild-type counterparts, CB6F1 mice and SD rats, were purchased from CLEA Japan Co., Ltd. (Tokyo, Japan). To confirm the results, CD-1 mice, which are frequently used in skin carcinogenesis studies, were also included in this series of studies. The animals were housed in the animal center of Nagoya City University Medical School, maintained on a 12 hr light-dark cycle and received Oriental MF basal diet (Oriental Yeast Co., Tokyo, Japan) and water *ad libitum*. All animals were kept for 1 week for acclimation. The experiments were conducted according to the Guidelines for the Care and Use of Laboratory Animals, and the study protocol was approved by the Institutional Animal Care and Use Committee of Nagoya City University Medical School.

Preparation of suspensions of titanium dioxide (TiO_2) and size analysis

$sTiO_2$ particles (silicone coated, mean manufacturer's particulate diameter of 35 nm) and $ncTiO_2$ particles (rutile type, mean manufacturer's particulate diameter of 20 nm) were provided by Japan Cosmetic Association, Tokyo, Japan. Size, coating, dose and suspension vehicles and animals used are summarized in Table 1. The size distribution of $sTiO_2$ suspended in silicone oil (cyclopentasiloxane, KF-995, Shin-Etsu Chemicals Co., Tokyo, Japan) or in saline and $ncTiO_2$ particles suspended in Pentalan 408 (pentaerythritol tetraethylhexanoate, CAS7299-99-2, Nikko Chemicals Co., Tokyo, Japan) or in saline was determined by a Particle Size Distribution Analyzer (Shimadzu Techno-Research Inc., Kyoto, Japan). The shape of suspended $sTiO_2$ and $ncTiO_2$ was observed by transmission electron microscopy (JEOL Co. Ltd., Tokyo, Japan). Freshly made suspensions were sonicated for 30 min, and suspensions were sonicated again for 30 min just prior to use.

Experimental design

Skin carcinogenesis study of silicone coated TiO_2 ($sTiO_2$) using rasH2 mice

The back skin of 7-week-old female rasH2 mice (60 mice) and wild-type CB6F1 mice (60 mice) was shaved (2 × 2 cm area) and the animals received a single topical application (painting) of 0.1 ml DMBA solution (2 mg/ml in acetone). Two weeks later, the animals were divided into 3 groups and the area which was painted with DMBA was shaved and painted with silicon oil alone or $sTiO_2$ suspended in silicon oil 5 times a week until termination of the experiment: Group 1 mice (15 mice of each strain) were painted with 0.2 ml silicone oil; group 2 mice (15 mice of each strain) were painted with 0.2 ml of 50 mg/ml $sTiO_2$ suspended in silicone oil; group 3 mice (15 mice of each strain) were painted with 0.2 ml of 100 mg/ml $sTiO_2$ suspended in silicone oil. Group 4 consisted of 15 mice of each strain painted with 0.2 ml 100 mg/ml $sTiO_2$ suspended in silicon oil 5 times a week without prior DMBA treatment. The rasH2 mice were killed at experimental week 8 and wild-type CB6F1 mice were killed at experimental week 40.

Skin carcinogenesis study of non-coated TiO_2 ($ncTiO_2$) using Hras128 rats

The back skin of 10-week-old male Hras128 rats (50 rats) and wild-type SD rats (36 rats) was shaved (3 × 3 cm area) and the animals received a single topical application (painting) of 0.5 ml DMBA solution (5 mg/ml in acetone)

(Park *et al.*, 2004). Two weeks later, the animals were divided into 3 groups and the area which was painted with DMBA was shaved and painted with Pentalan 408 alone or $ncTiO_2$ suspended in Pentalan 408 twice a week until termination of the experiment: Group 1 rats (17 Hras128 and 12 SD rats) were painted with 0.5 ml Pentalan 408 alone; group 2 rats (16 Hras128 and 12 SD rats) were painted with 0.5 ml of 100 mg/ml $ncTiO_2$ suspended in Pentalan 408; group 3 rats (17 Hras128 and 12 SD rats) were painted with 0.5 ml of 200 mg/ml $sTiO_2$ suspended in Pentalan 408. The Hras128 rats were killed at experimental week 28 and wild-type SD rats were killed at experimental week 40.

Skin carcinogenesis study of non-coated TiO_2 ($ncTiO_2$) using wild-type CD1 mice

The back skin of 10-week-old female CD1 mice (62 mice) was shaved (2 × 2 cm area) and the animals received a single topical application (painting) of 0.1 ml DMBA solution (2 mg/ml in acetone). Two weeks later, the animals were divided into 4 groups and the area which was painted with DMBA was shaved and painted with Pentalan 408 alone twice a week, $ncTiO_2$ suspended in Pentalan 408 twice a week, or TPA 4 times a week (positive control) until termination of the experiment: Group 1 mice (16 mice) were painted with 0.2 ml Pentalan 408; group 2 mice (16 mice) were painted with 0.2 ml of 50 mg/ml $ncTiO_2$ suspended in Pentalan 408; group 3 mice (15 mice) were painted with 0.2 ml of 100 mg/ml $ncTiO_2$ suspended Pentalan 408; group 4 mice (15 mice) were painted with 0.2 ml TPA solution (200 nmol/ml in acetone). Group 1-3 mice were killed at experimental week 52; group 4 mice were killed at experimental week 40.

Skin penetration study of non-coated TiO_2 ($ncTiO_2$) in SD rats

Based on our previous study showing lack of TiO_2 penetration through the normal skin (Xu *et al.*, 2011), $ncTiO_2$ was applied to damaged skin, which is postulated to be more susceptible to particle penetration. The back skin of 10-week-old female SD rats (24 rats) was shaved (3 × 3 cm area) and the epidermis was removed by stripping the epidermis off with a fresh piece of adhesive tape (3M's No. 3760, Scotch Mending Tape, Sumitomo 3M Ltd., Tokyo, Japan): Stripping was done 30 times to completely remove the epidermis. The epidermis-stripped skin was then painted with 0.5 ml of Pentalan or 0.5 ml of 200 mg/ml $ncTiO_2$ suspended in Pentalan 408 at 4-day-intervals over the course of 3 and a half weeks (7 treatments in 3½ weeks). Localization of $ncTiO_2$ particles in the epidermis was determined by histological observation. Skin tissue samples were taken at 1, 3, and 7 days after stripping to examine recovery of the epidermis and penetration of $ncTiO_2$ into the skin.

Skin penetration study of silicone coated TiO_2 ($sTiO_2$) in the in vitro skin model

To evaluate whether optimally dispersed $sTiO_2$ particles could penetrate into the epidermis, we applied $sTiO_2$ particles dispersed in silicone oil to the LabCyte EPI-MODEL kit (Japan Tissue Engineering Co. Ltd., Aichi, Japan), which is constructed of human skin epidermis keratinocytes on a mesh over a receiving chamber. In 12 wells: 4 wells had silicone oil alone applied directly to the human skin epidermis keratinocytes for 48 hr; 4 wells had 100 mg/ml $sTiO_2$ suspended in silicone oil applied directly to the human skin epidermis keratinocytes for 48 hr; and 4 wells had 200 mg/ml $sTiO_2$ suspended in silicone oil applied directly to the human skin epidermis keratinocytes for 48 hr. The medium in the receiving chamber was collected for elemental titanium analysis by an inductively coupled plasma/mass spectrometry (ICP-MS) (HP-4500, Hewlett-Packard Co., Houston,TX, USA) as described previously (Xu *et al.*, 2011).

Statistical analysis

Statistical analysis was performed using the Kruskal-Wallis and Bonferroni-Dunn's multiple comparison tests. Statistical significance was analyzed using a two-tailed Student's *t*-test and Bonferroni-Dunn's multiple comparison test. A value of $P < 0.05$ was considered to be significant.

RESULTS

Size distribution of $ncTiO_2$ and $sTiO_2$ particles

Transmission electron microscopy (TEM) analysis showed that the shape of $sTiO_2$ particles was generally round to oval (Fig. 1A), while $ncTiO_2$ particles were more clubbed shaped (Fig. 1B). The $sTiO_2$ in silicone oil solutions remained without obvious sedimentation for 3 days after preparation (Fig. 1C). In contrast, the $ncTiO_2$ in Pentalan 408 solutions contained considerable sedimentation 3 days after preparation (Fig. 1D). The particle size distribution of $sTiO_2$ and $ncTiO_2$ solutions is shown in Figs. 1E and 1F. The mean length of $sTiO_2$ particles suspended in saline and silicone was 0.16 ± 0.07 and 0.28 ± 0.22 μm, respectively (Fig. 1E). The mean length of $ncTiO_2$ particles suspended in saline and Pentalan 408 was 3.18 ± 0.35 and 4.97 ± 0.50 μm, respectively (Fig. 1F). These results indicate that $sTiO_2$ in silicone oil remained dispersed for a longer time than $ncTiO_2$ in Pentalan 408.

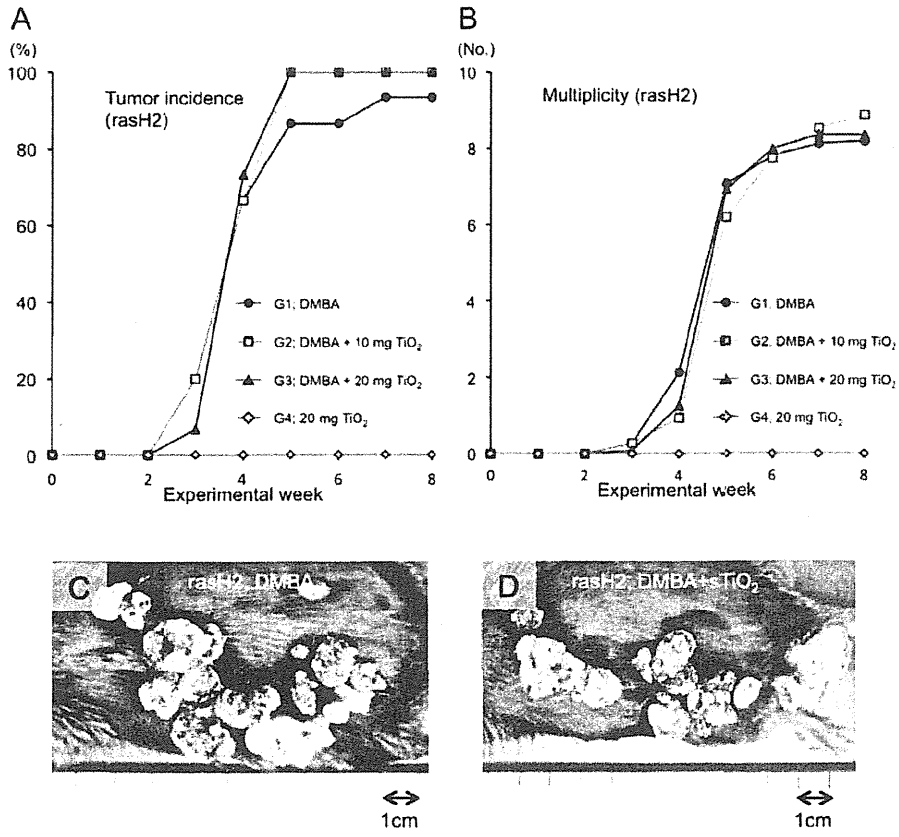

Fig. 2. Effects of $sTiO_2$ in a two-stage carcinogenesis model using rasH2 mice. The incidence of skin tumors in rasH2 mice: DMBA treated group (black circles), DMBA followed by treatment with 10 mg $sTiO_2$ (gray squares) or 20 mg $sTiO_2$ (black triangles). 20 mg $sTiO_2$ treated group (gray diamonds) (A). Multiplicity of skin tumors in rasH2 mice: DMBA treated group (black circles), DMBA followed by treatment with 10 mg $sTiO_2$ (gray squares) or 20 mg $sTiO_2$ (black triangles). 20 mg $sTiO_2$ treated group (gray diamonds) (B). Representative macroscopic appearance of skin tumors initiated with DMBA in rasH2 mice (C). The gross morphology of the tumors did not show obvious differences between the DMBA (C) and DMBA + $sTiO_2$ (D) groups.

Skin carcinogenesis study of $sTiO_2$ in silicone oil using rasH2 mice

Figures 2A and 2B show the time lapse incidence and multiplicity (number/mouse) of macroscopic skin tumors in rasH2 mice. No statistically significant differences were found between $sTiO_2$ treated rasH2 mice (groups 2 and 3: DMBA plus 50 mg/ml and 100 mg/ml $sTiO_2$, respectively) and control rasH2 mice (group 1: DMBA alone) (Figs. 2A and 2B, Table 2-1). Similarly, no statistically significant differences were found between treated and control groups of wild-type CB6F1 mice (Table 2-2). No tumors were induced in group 4 ($sTiO_2$ alone) of either rasH2 (Figs. 2A and 2B, Table 2-1) or wild-type CB6F1 mice (Table 2-2). Skin tumors were histologically SCP and SCC in rasH2 and wild-type CB6F1 mice. Representative macroscopic skin tumors induced by DMBA alone and by DMBA plus $sTiO_2$ are shown in Fig. 2C and 2D, respectively.

Skin carcinogenesis study of $ncTiO_2$ using Hras128 rat

Figures 3A and 3B show the time lapse incidence and multiplicity (number/rat) of macroscopic skin tumors in Hras128 rats. No statistically significant differences were found between $sTiO_2$ treated and control rasH2 rats (Figs. 3A and 3B, Table 3-1). Similarly, no statistically significant differences were found between treated and control groups of wild-type SD rats (Table 3-2).

Microscopically, TiO_2 was not observed within the SCP or SCC tissue (Figs. 4A and 4B). TiO_2 was observed

Table 2-1. Effects of $sTiO_2$ on skin carcinogenesis in rasH2 mice

Group	Treatment	No. of mice	SCP		SCC		SCP + SCC	
			Incidence (%)	Multiplicity	Incidence (%)	Multiplicity	Incidence (%)	Multiplicity
1	DMBA + Silicone	15	14 (93)	7.27 ± 4.74	5 (33)	0.60 ± 0.99	14 (93)	7.87 ± 5.17
2	DMBA + 10 mg TiO_2	15	15 (100)	8.13 ± 3.66	9 (60)	1.00 ± 1.00	15 (100)	9.13 ± 3.76
3	DMBA + 20 mg TiO_2	15	15 (100)	6.80 ± 3.88	8 (53)	0.73 ± 0.80	15 (100)	7.53 ± 3.31
4	20 mg TiO_2	15	0	0	0	0	0	0

SCP, squamous cell papilloma; SCC, squamous cell carcinoma.
Multiplicity: number of tumors per mouse.

Table 2-2. Effects of $sTiO_2$ on skin carcinogenesis in wild-type CB6F1 mice

Group	Treatment	No. of mice	SCP		SCC		SCP + SCC	
			Incidence (%)	Multiplicity	Incidence (%)	Multiplicity	Incidence (%)	Multiplicity
1	DMBA + Silicone	15	1 (7)	0.07 ± 0.26	1 (7)	0.07 ± 0.26	2 (13)	0.13 ± 0.35
2	DMBA + 10 mg TiO_2	15	2 (13)	0.13 ± 0.35	0	0	2 (13)	0.13 ± 0.35
3	DMBA + 20 mg TiO_2	15	2 (13)	0.20 ± 0.56	0	0	2 (13)	0.20 ± 0.56
4	20 mg TiO_2	15	0	0	0	0	0	0

SCP, squamous cell papilloma; SCC, squamous cell carcinoma.
Multiplicity: number of tumors per mouse.

on the surface and in the upper SC tissue and upper part of the hair follicles, but not in the underlying epidermis, dermis or subcutaneous tissues (Figs. 4C and 4D).

Skin carcinogenesis study of $ncTiO_2$ using wild-type CD1 mice

No statistically significant differences in tumor incidence or multiplicity was observed between treated and control groups of CD1 mice (Table 4). TPA treatment after DMBA significantly increased the incidence and multiplicity of SCP ($P < 0.001$).

Skin penetration study of $ncTiO_2$ in SD rats

Figures 5 A-D shows skin tissue samples collected before (Fig. 5A) and 1, 3 and 7 days after (Figs. 5B-D) removing the epidermis by tape-stripping. On day 1 the epidermis was completely removed (Fig. 5B), and a mass of fibrin exudate and underlying granulation tissue rich with neutrophils was the main feature of the skin surface. On day 3, regenerated epidermis already covered the granulation tissue (Fig. 5C). On day 7, the surface of the skin was fully covered by regenerated keratinocytes showing cornification and had an almost normal appearance (Fig. 5D).

The shaved back skin of SD-rats was painted with 100 mg TiO_2 suspended in Pentalan 408. Fig. 5E shows the presence of $ncTiO_2$ particles in the SC layer of the skin of these animals. Extensive histological observation failed to detect TiO_2 within the epidermis or dermis. In another series of experiments, the epidermis was removed from the back skin of SD rats by tape-stripping and the freshly stripped skin was painted with 100 mg $ncTiO_2$ suspended in Pentalan 408. This was repeated every 4 days for 3½ weeks (7 times total). Figure 5F shows the presence of TiO_2 on the surface of the regenerating epidermis 1 day after the last stripping/painting procedure. Extensive

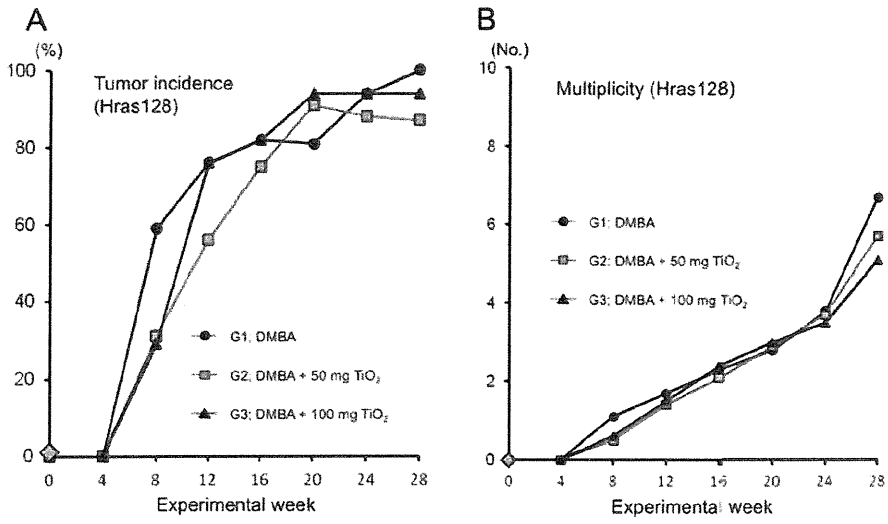

Fig. 3. Effects of $ncTiO_2$ in a two-stage carcinogenesis model using Hras128 rats. The incidence of skin tumors in Hras128 rats: DMBA treated group (black circles), DMBA followed by treatment with 50 mg $ncTiO_2$ (gray squares) or 100 mg $ncTiO_2$ (black triangles) (A). Multiplicity of skin tumors in rasH2 mice: DMBA treated group (black circles), DMBA followed by treatment with 100 mg $ncTiO_2$ (gray squares) or 200 mg $ncTiO_2$ (black triangles) (B).

Table 3-1. Effects of $ncTiO_2$ on skin carcinogenesis in Hras128 rats

Group	Treatment	No. of rats	SCP		SCC		SCP + SCC	
			Incidence (%)	Multiplicity	Incidence (%)	Multiplicity	Incidence (%)	Multiplicity
1	DMBA + Pentalan 408	17	16 (94)	9.65 ± 7.05	0	0	16 (94)	9.65 ± 7.05
2	DMBA + 50 mg TiO_2	16	14 (88)	6.81 ± 6.21	2 (13)	0.19 ± 0.54	14 (88)	7.00 ± 6.52
3	DMBA + 100 mg TiO_2	17	16 (94)	7.59 ± 3.86	2 (12)	0.12 ± 0.331	16 (94)	7.71 ± 3.93

SCP, squamous cell papilloma; SCC, squamous cell carcinoma.
Multiplicity: number of tumors per rat.

Table 3-2. Effects of $ncTiO_2$ on skin carcinogenesis in wild-type SD rats

Group	Treatment	No. of rats	SCP		SCC		SCP + SCC	
			Incidence (%)	Multiplicity	Incidence (%)	Multiplicity	Incidence (%)	Multiplicity
1	DMBA + Pentalan 408	12	3 (25)	0.25 ± 0.45	0	0	3 (25)	0.25 ± 0.45
2	DMBA + 50 mg TiO_2	12	2 (17)	0.17 ± 0.39	2 (17)	0.17 ± 0.39	4 (33)	0.33 ± 0.49
3	DMBA + 100 mg TiO_2	12	1 (8)	0.08 ± 0.29	0	0	1 (8)	0.08 ± 0.29

SCP, squamous cell papilloma; SCC, squamous cell carcinoma.
Multiplicity: number of tumors per rat.

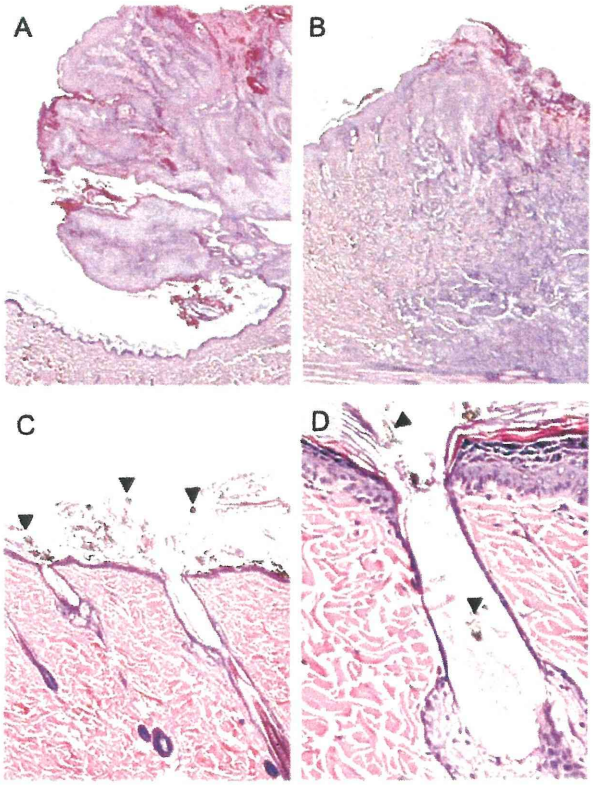

Fig. 4. Effects of $ncTiO_2$ in a two-stage carcinogenesis model. Representative histological features of SCP (A) and SCC (B) on the back skin of a Hras128 rat. TiO_2 aggregates were seen on the surface of stratum corneum (C, arrowheads), but not in the underlying epidermis, dermis or subcutaneous tissue. Some aggregates were found in the upper layer of stratum corneum (arrowheads) and in the lumen of the hair follicle (D) but not in the dermis.

histological observation failed to detect any TiO_2 particles in the underlying epidermis or dermis, indicating that $ncTiO_2$ failed to penetrate into the stripped skin. In addition, no inflammatory lesions were found in the epidermis or subcutaneous tissue of these animals. These results indicate that TiO_2 particles do not penetrate into the epidermis of either normal or damaged skin.

In vitro skin penetration study

The amount of elemental titanium in the receiving chamber did not show any significant increase over the vehicle group (Table 5). All the observed values are equivalent to background. The results indicate that $sTiO_2$ particles did not penetrate the human epidermis in this model.

DISCUSSION

TiO_2 particles, including both nano and larger sized particles, are known to be carcinogenic to the rat lung (Baan *et al.*, 2006). We have shown that alveolar macrophages play an important role in promotion of lung carcinogenesis when TiO_2 particles are inhaled into the lung (Xu *et al.*, 2011). Because of this, TiO_2 particles, especially nano-sized particles, are deemed to have the potential to induce skin tumors after long-term topical application should the particles penetrate into the epidermis and subcutaneous tissue and interact with macrophages. The current study is the first systematic study of the skin promotion/carcinogenesis effects of TiO_2 in a two-stage chemical carcinogenesis animal model. We found that even the smallest available sized TiO_2 ($sTiO_2$) did not exhibit promoting effects on the highly sensitive rasH2 mouse skin carcinogenesis model. Furthermore, we observed that TiO_2 without coating ($ncTiO_2$) did not cause skin tumor promotion in the skin carcinogenesis-sensitive Hras128 rat model or in the CD1 mouse. These results are in agreement with another recent study reporting the lack of carcinogenicity of topically applied TiO_2 (Furukawa *et al.*, 2011).

We also found that topically applied $ncTiO_2$ did not penetrate normal rat skin or skin which had the epidermis completely removed, nor did $sTiO_2$ penetrate the *in vitro* human epidermis model. Thus, the lack of skin promotion/carcinogenesis effects is probably due to lack of penetration of the particles through the epidermis to the dermis where cytogenetic cells of skin carcinogenesis reside. In another study, we found no promoting effect of TiO_2 particles in a UVB-initiated long-term (52 weeks) skin carcinogenesis study and no penetration of TiO_2 particles through the epidermis (Xu *et al.*, 2011).

Results showing lack of TiO_2 penetration through the epidermis are in accordance with other reports. Numerous *in vitro* and *in vivo* studies using murine, porcine, or human skin have shown that nano-sized TiO_2 does not penetrate the skin (reviewed in Nohynek *et al.* (2008)). In addition to these studies, Gottbrath *et al.* (2003) report that after topical application of TiO_2 to the underside of the forearm of a human volunteer, ultrafine TiO_2 did not penetrate beyond the SC.

Contrary to these findings, there is a single report by Wu *et al.* (2009) that TiO_2 particles (4 and 60 nm) did penetrate into the deep layers of the epidermis after topical application to the pig ear for 30 days (Wu *et al.*, 2009). They also reported that nano-size TiO_2 particles could penetrate the skin of hairless mice after 60 days dermal exposure, although they did not examine promotion/car-

Table 4. Effects of $ncTiO_2$ on skin carcinogenesis in wild-type CD1 mice

Group	Treatment	No. of mice	SCP		SCC		SCP + SCC	
			Incidence (%)	Multiplicity	Incidence (%)	Multiplicity	Incidence (%)	Multiplicity
1	DMBA + Pentalan 408	16	3 (19)	0.25 ± 1.30	0	0	3 (19)	0.25 ± 0.58
2	DMBA + 10 mg TiO_2	16	1 (6)	0.06 ± 0.25	0	0	1 (6)	0.06 ± 0.25
3	DMBA + 20 mg TiO_2	15	2 (13)	0.13 ± 0.35	0	0	2 (13)	0.13 ± 0.35
4	DMBA + TPA	15	13 (87)*	2.00 ± 1.41*	2 (13)	0.13 ± 0.35	13 (87)*	2.00 ± 1.41*

* Significantly different from group 1 (control) by Student's t-test ($p < 0.001$).
SCP, squamous cell papilloma; SCC, squamous cell carcinoma.
Multiplicity: number of tumors per mouse.

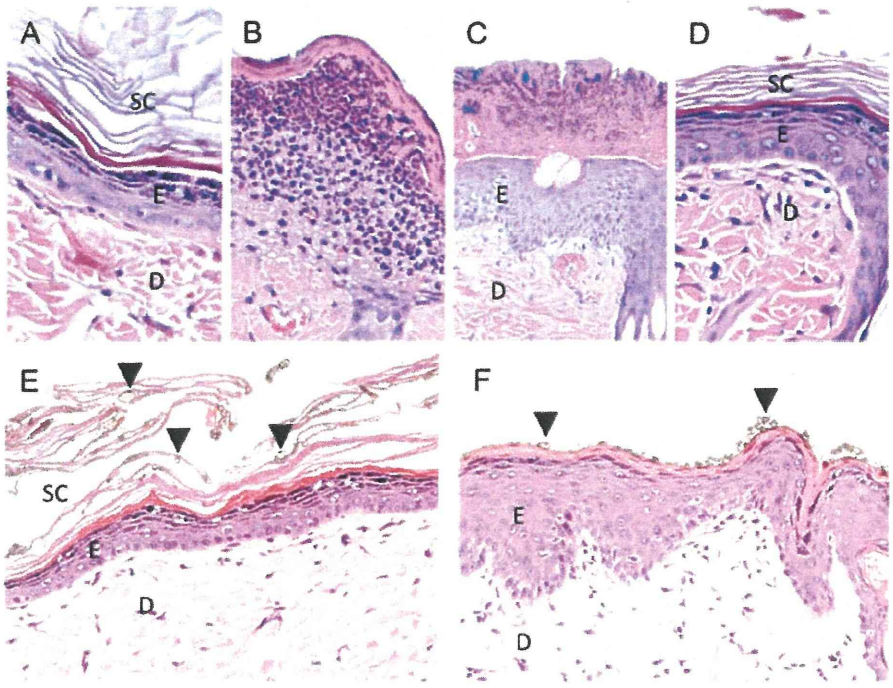

Fig. 5. Histological features of the skin after striping away the epidermis and study of $ncTiO_2$ penetration into normal and stripped skin using wild-type Sprague-Dawley rats. The back skin of SD rats was shaved and the epidermis was left intact or stripped away using tape. Stratum corneum (SC), epidermis (E), and dermis (D) are intact in the shaved, not stripped group (A). In the tape-stripped group, one day after stripping away the epidermis, the stripping site is covered with fibrin exudates with rich neutrophilic infiltration (B). Three days after stripping, regenerated epidermis (E) is present underneath the exudate (C). Seven days after stripping, the regenerated epidermis (E) is composed of mature keratinocytes and a stratum corneum (SC) (D). The back skin of SD rats was shaved (but the epidermis was not stripped away) and painted with $ncTiO_2$ suspended in Pentalan 408. $ncTiO_2$ aggregates are present in the stratum corneum (SC) (arrowheads, brown material) of the skin of these animals (E); particles were not detected within the underlying skin tissue. Freshly stripped skin was painted with $ncTiO_2$ suspended in Pentalan 408, and this process was repeated every 4 days over the course of $3^1/_2$ weeks (7 times total). $ncTiO_2$ particles (arrowheads, brown material) are present on the surface of the skin one day after the last stripping/painting procedure (F); particles were not detected in the underlying tissue.

Table 5. *In vitro* penetration of $sTiO_2$ particles

Treatment	Amount of elemental titanium in the receiving chamber (μg/ml)
Silicone oil	0.11 ± 0.01
100 mg/ml $sTiO_2$	0.14 ± 0.01
200 mg/ml $sTiO_2$	0.12 ± 0.01
None	0.11 ± 0.03

cinogenesis effects of the particles (Wu *et al.*, 2009). Differences in experimental systems (i.e., animal strain used in the experiment, exposure period, particle suspension, mean primary/actual length of the particle, and TiO_2 manufacturer) may possibly explain the discrepancies reported on TiO_2 particle penetration.

Two studies have reported finding TiO_2 particles in hair follicles (Bennat and Muller-Goymann, 2000; Lekki *et al.*, 2007). These studies taken together with Wu *et al.* (2009) suggest the possibility that the hair follicle may be a route of skin penetration by TiO_2 particles. However, we found that TiO_2 particles remained primarily in the SC and the upper lumen of hair follicles. Bennat and Muller-Goymann (2000) and Lekki *et al.* (2007) also report that while topically applied TiO_2 was found in hair follicules, it did not penetrate into the underlying tissue or sebaceous glands.

Penetration of TiO_2 into underlying dermal tissues even after removing the entire epidermis by tape-stripping did not occur. Rather, aggregates of TiO_2 particles were found on the exterior of the SC exhibiting regeneration and no particles were found in the underlying tissues. The freshly manufactured TiO_2 particles used in the present study primarily measured 20-35 nm in their longer diameter. These particles are lyophobic and easily form micro-sized aggregates (160-5,000 nm in length), and these larger particles are unable to penetrate through the epidermis.

In summary, nano-sized TiO_2 particles, even silicone coated TiO_2 suspended in silicone oil which provides optimal dispersion of the particles, did not penetrate the epidermis of rat or human skin models and did not exhibit promoting effects in rat or mouse two-stage skin carcinogenesis models. Therefore, topical application of TiO_2 was not carcinogenic, and this lack of carcinogenicity is likely due to the lack of penetration through the epidermis. Our studies taken together with other reports lead us to conclude that topical application of TiO_2 to human skin is very unlikely to pose a potential risk to human health.

ACKNOWLEDGMENTS

This work was supported by Health and Labour Sciences Research Grants (Research on Risk of Chemical Substance, H19-kagaku-ippan-006 and H22-kagaku-ippan-005), and Grant-in aid for cancer research from the Ministry of Health, Labour and Welfare, Japan.

REFERENCES

Baan, R., Straif, K., Grosse, Y., Secretan, B., El Ghissassi, F. and Cogliano, V. (2006): Carcinogenicity of carbon black, titanium dioxide, and talc. Lancet Oncol., **7**, 295-296.

Baan, R.A. (2007): Carcinogenic hazards from inhaled carbon black, titanium dioxide, and talc not containing asbestos or asbestiform fibers: recent evaluations by an IARC Monographs Working Group. Inhal. Toxicol., **19**, 213-228.

Bennat, C. and Muller-Goymann, C.C. (2000): Skin penetration and stabilization of formulations containing microfine titanium dioxide as physical UV filter. Int. J. Cosmet. Sci., **22**, 271-283.

Furukawa, F., Doi, Y., Suguro, M., Morita, O., Kuwahara, H., Masunaga, T., Hatakeyama, Y. and Mori, F. (2011): Lack of skin carcinogenicity of topically applied titanium dioxide nanoparticles in the mouse. Food Chem. Toxicol., **49**, 744-749.

Gelis, C., Girard, S., Mavon, A., Delverdier, M., Paillous, N. and Vicendo, P. (2003): Assessment of the skin photoprotective capacities of an organo-mineral broad-spectrum sunblock on two ex vivo skin models. Photodermatol. Photoimmunol. Photomed., **19**, 242-253.

Gottbrath, S, C.M.-G. (2003): Penetration and visualization of titanium dioxide microparticles in human stratum corneum-effect of different formulations on the penetration of titanium dioxide. SOFW Journal, **129**, 11-17.

Lekki, J., Stachura, Z., Dąbroś, W., Stachura, J., Menzel, F., Reinert, T., Butz, T., Pallon, J.. Gontier, E., Ynsa, M.D., Moretto, P., Kertesz, Z., Szikszai, Z. and Kiss, A.Z. (2007): On the follicular pathway of percutaneous uptake of nanoparticles: Ion microscopy and autoradiography studies. Nucl. Instrum. Methods Phys. Res., Section B, **260**, 174-177.

Muto, S., Katsuki, M. and Horie, S. (2006): Rapid induction of skin tumors in human but not mouse c-Ha-ras proto-oncogene transgenic mice by chemical carcinogenesis. Cancer Sci., **97**, 842-847.

Newman, M.D., Stotland, M. and Ellis, J.I. (2009): The safety of nanosized particles in titanium dioxide- and zinc oxide-based sunscreens. J. Am. Acad. Dermatol., **61**, 685-692.

Nohynek, G.J., Dufour, E.K. and Roberts, M.S., (2008): Nanotechnology, cosmetics and the skin: is there a health risk? Skin. Pharmacol. Physiol., **21**, 136-149.

Park, C.B., Fukamachi, K., Takasuka, N., Han, B.S., Kim, C.K., Hamaguchi, T., Fujita, K., Ueda, S. and Tsuda, H. (2004): Rapid induction of skin and mammary tumors in human c-Ha-ras proto-oncogene transgenic rats by treatment with 7,12-dimethylbenz[a] anthracene followed by 12-O-tetradecanoylphorbol 13-acetate. Cancer Sci., **95**, 205-210.

Rouabhia, M., Mitchell, D.L., Rhainds, M., Claveau, J. and Drouin, R. (2002): A physical sunscreen protects engineered human skin against artificial solar ultraviolet radiation-induced tissue and DNA damage. Photochem. Photobiol. Sci., **1**, 471-477.

Schaefer, H., Redelmaier, T. and Nohynek, G. (2003): Pharmacok-

inetics and topical application of drugs. In Fitzpatrick's Dermatology in General Medicine (Freedberg, I., Eisen, A., Wolff, K., Austen, F., Goldsmith, L. and Katz, S. eds.), pp.2313-2318, McGraw-Hill, New York.

Senzui, M., Tamura, T., Miura, K., Ikarashi, Y., Watanabe, Y. and Fujii, M. (2010): Study on penetration of titanium dioxide (TiO(2)) nanoparticles into intact and damaged skin in vitro. J. Toxicol. Sci., **35**, 107-113.

Suzuki, M. (1987): Protective effect of fine-particle titanium dioxide on UVB-induced DNA damage in hairless mouse skin. Photodermatol., **4**, 209-211.

Wu, J., Liu, W., Xue, C., Zhou, S., Lan, F., Bi, L., Xu, H., Yang, X. and Zeng, F.D. (2009): Toxicity and penetration of TiO2 nanoparticles in hairless mice and porcine skin after subchronic dermal exposure. Toxicol. Lett., **191**, 1-8.

Xu, J., Sagawa, Y., Futakuchi, M., Fukamachi, K., Alexander, D.B., Furukawa, F., Ikarashi, Y., Uchino, T., Nishimura, T., Morita, A., Suzui, M. and Tsuda, H. (2011): Lack of promoting effect of titanium dioxide particles on ultraviolet B-initiated skin carcinogenesis in rats. Food Chem. Toxicol., **49**, 1298-1302.

Xu, J., Futakuchi, M., Iigo, M., Fukamachi, K., Alexander, DB., Shimizu, H., Sakai, Y., Tamano, S., Furukawa, F., Uchino, T., Tokunaga, H., Nishimura, T., Hirose, A., Kanno, J. and Tsuda, H. (2010): Involvement of macrophage inflammatory protein 1alpha (MIP1alpha) in promotion of rat lung and mammary carcinogenic activity of nanoscale titanium dioxide particles administered by intra-pulmonary spraying. Carcinogenesis, **31**, 927-935.

Toxicology Letters 206 (2011) 172–177

Contents lists available at ScienceDirect

Toxicology Letters

journal homepage: www.elsevier.com/locate/toxlet

Time-dependent variation in the biodistribution of C_{60} in rats determined by liquid chromatography–tandem mass spectrometry

Reiji Kubota[a,*], Maiko Tahara[a], Kumiko Shimizu[a], Naoki Sugimoto[a], Akihiko Hirose[b], Tetsuji Nishimura[a]

[a] Division of Environmental Chemistry, National Institute of Health Sciences, Kamiyoga 1-18-1, Setagaya-ku, Tokyo 158-8501, Japan
[b] Division of Risk Assessment, Biological Safety Research Center, National Institute of Health Sciences, Kamiyoga 1-18-1, Setagaya-ku, Tokyo 158-8501, Japan

ARTICLE INFO

Article history:
Received 7 June 2011
Received in revised form 8 July 2011
Accepted 8 July 2011
Available online 20 July 2011

Keywords:
Fullerenes
Tissue distribution
Rat
LC–MS/MS
Nanoparticles

ABSTRACT

We examined the biodistribution of C_{60} in rats after tail vein administration using LC–MS/MS. C_{60} was detected in various tissues, such as brain, kidneys, liver, lungs, and spleen of rats. On the other hand, no C_{60} was found in blood. The highest C_{60} concentration was observed in the lungs, followed by spleen, liver, kidneys, and brain. These results suggested that C_{60} injected in the tail vein could be filtered by lung capillary vessels and accumulate in the lungs prior to being distributed to other tissues. Moreover, C_{60} not being detected in the blood indicates that clearance of C_{60} from the blood by filtration might effectively occur in the lungs. The time-dependent variation in the biodistribution of C_{60} was evaluated. A time-dependent decrease in C_{60} concentrations was observed in all tissues, except spleen. Moreover, a decreasing trend of C_{60} levels differed among tissues, which could be due to differences in accumulation. These results suggest that unmodified C_{60} and/or C_{60} metabolites by metabolic enzymes could be excreted into feces and/or urine. In further studies, the metabolic and excretion pathways of C_{60} should be evaluated to understand the toxicokinetics of C_{60}.

1. Introduction

Recent progress in the field of nanotechnology has resulted in the development of various newly engineered nanomaterials. Engineered nanomaterials are commonly produced in a wide variety of types, including fullerenes (C_{60}), carbon nanotubes (CNT), metal and metal oxide particles, polymer nanoparticles, and quantum dots. These materials have been applied to various fields of science and technology, and have increasingly been used for commercial purposes, such as fillers, opacifiers, catalysts, semiconductors, and personal care products (cosmetics and drugs) (Nel et al., 2006). On the other hand, there is insufficient information about the human health and environmental impact of nanomaterials, and concern about exposure to nanomaterials and the hazard that they pose is rising (Colvin, 2003; Moore, 2006).

Fullerene, a carbon nanomaterial, is a third allotropic form of carbon (after graphite and diamond). Unlike other carbon structures, fullerene is a closed cage carbon molecule with a truncated icosahedron structure that resembles a soccer ball with 12 pentagons and 20 hexagons (Kroto et al., 1985). Because of their unique structures and properties, fullerenes and their derivatives (endohedral fullerenes and chemically modified fullerenes) exhibit widely differing activities and therefore have attracted considerable attention. Since the water solubility of unmodified C_{60} is low, several studies have been performed to increase its water solubility by surface chemical modification and the formation of complexes with water soluble molecules (Bosi et al., 2003; Nakamura and Isobe, 2003), and as a result of these studies, a number of biological applications, such as free radical scavengers (Dugan et al., 1997), photoinduced DNA cleavage agents (Tokuyama et al., 1993), inhibitors of HIV-1 protease (Friedman et al., 1993), and cytotoxic agents to human cells (HDF, HepG2, and NHA) by lipid peroxidation (Sayes et al., 2005), for fullerene derivatives have been discovered. Rapid commercialization of fullerenes and their derivatives has increased the risk of occupational and environmental human exposure to these nanomaterials via oral, dermal, and inhalation uptake. However, little is known about the potential impact induced by exposure to nanomaterials (fullerenes and their derivatives) to human health, and comprehensive studies on the toxicology and biodistribution of fullerenes and their derivatives have been insufficient. To accurately evaluate the toxic effects of fullerenes and their derivatives by *in vivo* and *in vitro* assays, it is necessary to use an analytical chemical approach coupled with a biological approach. Several methods for analyzing fullerenes and their derivatives have been reported. However, only a few studies have

* Corresponding author. Tel.: +81 3 3700 9346; fax: +81 3 3700 9346.
E-mail address: reijik@nihs.go.jp (R. Kubota).

0378-4274/$ – see front matter © 2011 Elsevier Ireland Ltd. All rights reserved.
doi:10.1016/j.toxlet.2011.07.010

examined fullerenes and their derivatives in biological samples (Moussa et al., 1997; Xia et al., 2006), and the sensitivity of detection was insufficient and there was interference from the biological matrix in the analysis of samples. Several studies have investigated the biodistribution of fullerenes in rodents (Yamago et al., 1995; Cagle et al., 1999). However, the fullerenes used in these studies were water-soluble fullerene derivatives, and physical properties of these derivatives differ significantly from unmodified fullerene, especially water solubility; thus, it would be expected that the biodistribution characteristics of modified fullerene derivatives would also differ from unmodified fullerene. Furthermore, there are very few reports on the biodistribution of unmodified fullerene (including radiolabeled fullerene, such as ^{14}C-labeled C_{60} where the label is part of the C_{60} cage) (Bullard-Dillard et al., 1996) in rodents. In this study, we describe the biodistribution of unmodified C_{60} in rats after tail vein administration using a sensitive liquid chromatography–tandem mass spectrometry (LC–MS/MS) analytical method and liposomes as a carrier of unmodified C_{60}. Liposomes are known as one of the most effective drugs carrier. Moreover, the time-dependent biodistribution variation of unmodified C_{60} in rats was investigated, and the behavior of C_{60} after accumulated in tissues is discussed.

2. Methods

2.1. Chemicals and reagents

C_{60} (nanom purple SUH; purity >99.9%) was obtained from Frontier Carbon Corporation (Tokyo, Japan). C_{70} with a purity of 99.5% was purchased from Materials Technologies Research (Cleveland, USA). C_{70} was used for recovery correction of C_{60} extraction. HPLC grade acetonitrile and toluene were purchased from Wako Pure Chemical Industries, Ltd. (Osaka, Japan). Analytical grade acetic acid, disodium hydrogen phosphate, potassium chloride, potassium dihydrogen phosphate, sodium chloride, sodium dodecylsulfate, and chloroform were also purchased from Wako Pure Chemical Industries, Ltd. (Osaka, Japan). L-α-Phosphatidyl-choline and 3-sn-phosphatidyl-L-serine were purchased from Sigma–Aldrich (St. Louis, USA). Stock standard solutions were prepared by dissolving C_{60} (10 mg) and C_{70} (10 mg) in toluene (10 mL) with sonication and agitation and were stored at −20 °C until use. Working standard solutions were diluted with toluene from stock standard solution for the LC–MS/MS analysis.

2.2. Instrumentation

LC–MS/MS analysis was performed using a Waters Alliance 2695 HPLC system (Waters, Milford, USA) interfaced to a Waters Micromass Quattro Micro API triple quadrupole mass spectrometer equipped with an atmospheric pressure chemical ionization (APCI) interface (Waters, Milford, USA). System control and data handling were carried out by Waters MassLynx version 4.0.

2.3. Chromatographic and mass spectrometric conditions

Analysis of C_{60} was conducted as described previously (Kubota et al., 2009). The chromatographic separation was performed in isocratic mode at a flow rate of 1 mL/min with a mobile phase of 70% toluene and 30% acetonitrile. Fullerenes were separated using a Develosil RPFULLERENE column (5 μm, 4.6 mm × 250 mm) (Nomura Chemical Co., Ltd., Seto, Japan) at 30 °C (column oven temperature). The autosampler was kept at 10 °C and the injection volume was 20 μL. The mass spectrometer was operated in the APCI negative ion mode with multiple reaction monitoring (MRM). The APCI corona current was 15 μA, and the temperatures of the source and APCI probe were set to 120 °C and 400 °C, respectively. The desolvation and the cone gas flow rates were adjusted to 600 L/h and 50 L/h, respectively. The inter-scan delay was set to 0.1 s, and the inter-channel delay was set to 0.05 s. The dwell time was 0.5 s. Quantitation was performed using MRM of the reaction transitions of m/z = Q1 720 → Q3 720 for C_{60} and m/z = Q1 840 → Q3 840 for C_{70} (used for recovery correction of C_{60} extraction) with a collision energy of 60 eV and a cone voltage of 120 V. Multiple reaction monitoring (MRM) chromatogram of a 200 μg/L standard mixture of C_{60} and C_{70} was shown in Fig. 1.

2.4. Experimental animals

20 male Wistar rats (Slc: Wistar (SPF)) were purchased from Japan SLC, Inc. (Shizuoka, Japan) at six weeks of age. The rats were kept under Specific Pathogen Free (SPF) conditions with a 12 h light–dark cycle at the animal facility of the National Institute of Health Sciences (NIHS), Tokyo, Japan and were given tap water and autoclaved CRF-1 pellets (Oriental Yeast Co., Ltd., Tokyo, Japan) *ad libitum*. Experiments were humanely conducted under the regulation and permission of the Animal Care and Use Committee of NIHS.

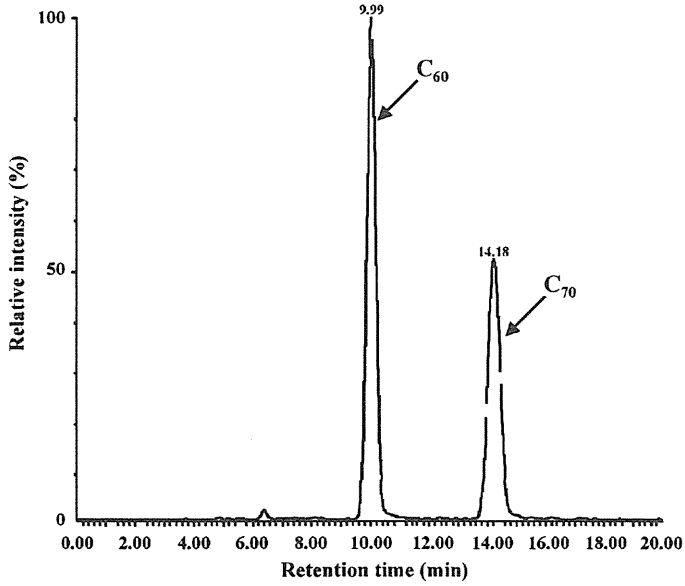

Fig. 1. Multiple reaction monitoring (MRM) chromatogram of a 200 μg/L mixture of C_{60} and C_{70}. Retention times (min) from top: C_{60} (9.99) and C_{70} (14.18).

2.5. Preparation of administration solution (C_{60}-liposome solution)

Because of the solubility of unmodified C_{60} is low, we used liposomes as a carrier of unmodified C_{60}. An administration solution for tail vein injection in rats was prepared as follows. L-α-Phosphatidyl-choline (PC) and 3-sn-phosphatidyl-L-serine (PS) were dissolved in chloroform as 25 mg/mL stock solutions and were stored at −80 °C until use. C_{60} was dissolved in toluene as a 2.5 mg/mL stock solution and was stored at 4 °C until use. A PC and PS mixture was prepared such that each component had a concentration of 0.5 mg/mL (PC:PS = 1:1 (w/w)) in chloroform. 1 mg/mL C_{60} solution (mixture of toluene and chloroform) was prepared by diluting the 2.5 mg/mL C_{60} stock solution with the lipid mixture and the mixture was gently volatilized with a stream of nitrogen gas. After volatilization, 1× PBS buffer (pH 7.4), an amount equivalent to the mixture of toluene and chloroform, was added, and the mixture was vortexed for a few seconds. The liposomes containing C_{60} were sonicated using a bath sonicator for 10–15 min at 60 °C and were centrifuged at 1000 rpm for 10 s, and the supernatant (at room temperature) was used for tail vein administration. The supernatant was given to rats immediately and the solution was sonicated using a bath sonicator before each treatment to rats.

2.6. Treatment of experimental animals and sample collection

20 male Wistar rats at six weeks of age (five per group) were given repeated tail vein injections of 5 mL/kg body weight (one injection). A total of four tail vein injections (once per day) were performed (total injected C_{60}: ca. 929.1 μg). Rats were sacrificed on days 1, 7, 14, and 28 after completion of the injections. Brain, kidneys, liver, lungs, and spleen were collected from each rat and were rinsed with 1 × PBS buffer (pH 7.4). Moreover, blood (taken from the heart) was collected from each rat group. The collected tissues and blood samples were stored at −80 °C until analyzed.

2.7. Sample preparation

Extraction of C_{60} from tissues and blood of rats was performed according to the method of Kubota et al. (2009) with modifications. Freshly harvested whole tissues were weighted and placed in polypropylene copolymer (PPCO) centrifuge tubes. Tissues were frozen at −80 °C, and frozen tissues were freeze-dried over night. Each freeze-dried tissue was weighted and completely homogenized. In the case of small tissues (<0.5 g dry wt., brain, kidneys, spleen, and lungs), 0.2 M SDS solution (1 mL) and acetic acid (1 mL) were added to the centrifuge tubes, and the centrifuge tubes were vortexed and sonicated using a bath sonicator. An internal standard solution (C_{70} toluene solution, 0.5 mL) and 3.5 mL toluene were added to the centrifuge tubes, and they were shaken for 5 h at room temperature in the dark. After shaking, the centrifuge tubes were centrifuged for 30 min at 3500 rpm. 1 mL of supernatant was removed and placed in glass vials to be used for analysis. In the case of blood samples, untreated whole blood (2 mL, taken from the heart) was used for the extraction. Because the dry tissue weight of the liver (ca. 3 g dry wt.) was heavier than other tissues, a six-fold amount of each solution was used for the liver extraction. The limit of quantification (LOQ) in analytical solution was determined by analyzing

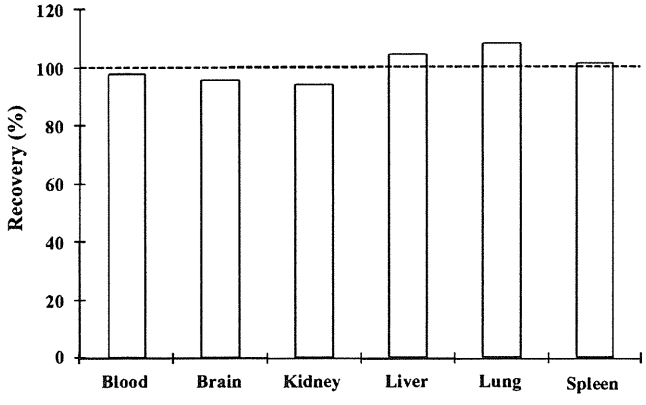

Fig. 2. Recovery of C_{60} from tissues and blood of rat.

the lowest level standard at least 5 times. The LOQ was calculated as 10-fold the standard deviation of these determinations. The LOQ value in analytical solution was 10 μg/L. Moreover, LOQ in each tissue was calculated by LOQ value in analytical solution, volume of toluene used for extraction, and tissue weight of each tissue. The LOQ for each tissue was 0.026 μg/g wet wt. for liver, 0.026 μg/g wet wt. for kidneys, 0.09 μg/g wet wt. for spleen, 0.046 μg/g wet wt. for lungs, and 0.023 μg/g wet wt. for brain, respectively.

2.8. Statistical analyses

Statistical analyses were performed using the program Excel Statistics (Ekuseru-Toukei 2008) (Social Survey Research Information Co., Ltd., Tokyo, Japan). Kolmogorov–Smirnov's test showed that some variables were not normally distributed. Therefore, non-parametric test was used for statistical analysis. Kruskal–Wallis test was used for validation of difference in the C_{60} concentrations in four tissues among treated groups. Where appropriate, Mann–Whitney's *U*-test, Scheffe's test, or Student's *t*-test was conducted to verify the difference in the C_{60} concentration in four tissues among each treated group.

3. Results

3.1. Recovery of C_{60} from tissues and blood of rat

A spike recovery test was conducted to evaluate the validity of the analytical method for determination of C_{60} in the tissues and blood of rat (Fig. 2). The recovery of C_{60} was determined by spiking samples collected from untreated rat. No C_{60} was observed in tissues and blood of untreated rat. 8 μL of C_{60} toluene solution (10 mg/L) was added to previously treated (tissues were freeze-dried, homogenized, added 0.2 M SDS and acetic acid, vortexed and sonicated.) tissues and blood (whole blood) giving a 20 μg/L final concentration, and was mixed. Thereafter, internal standard solution (toluene) and toluene were added and subsequent processes were conducted as described in Section 2. The recovery percentage was calculated by comparing the sample peak areas with those of the C_{60} standard solution at the same concentration (final concentration: 20 μg/L). Recovery percentages of C_{60} were 98.1% for blood, 95.7% for brain, 94.0% for kidneys, 105.0% for liver, 108.3% for lungs, and 101.4% for spleen, respectively. In the case of all tissues and blood as well as the internal standard, good recoveries were obtained. These results suggested that our method was valid for determining C_{60} concentrations in biological samples.

3.2. C_{60} concentrations in five tissues and blood of rats

C_{60} concentrations in tissues and blood of rats after tail vein injection were determined. Although no C_{60} was detected in the blood, C_{60} was observed in almost all of the tissues examined in this study (Table 1). For the Day 1 and Day 7 groups, C_{60} was detected in all samples from the five collected tissues of rats. C_{60} concentrations (mean ± SD) in tissues of the Day 1 rat group were 254 ± 114 μg/g wet wt. for lungs, 53.0 ± 18.8 μg/g wet wt. for spleen, 25.5 ± 5.56 μg/g wet wt. for liver, 1.30 ± 0.68 μg/g wet wt. for kidneys, and 0.08 ± 0.01 μg/g wet wt. for brain. C_{60} concentrations (mean ± SD) in tissues of the Day 7 rat group were 199 ± 88.4 μg/g wet wt. for lungs, 45.3 ± 10.7 μg/g wet wt. for spleen, 22.6 ± 9.63 μg/g wet wt. for liver, 0.42 ± 0.11 μg/g wet wt. for kidneys, and 0.04 ± 0.01 μg/g wet wt. for brain. For the Day 14 and Day 28 groups, although C_{60} was detected in all samples of the lungs, spleen, liver, and kidneys, C_{60} was only detected in one specimen of the Day 14 group in brain tissue. C_{60} concentrations (mean ± SD) in tissues of the Day 14 rat group were 109 ± 51.5 μg/g wet wt. for lungs, 59.0 ± 14.4 μg/g wet wt. for spleen, 21.9 ± 4.94 μg/g wet wt. for liver, 0.20 ± 0.02 μg/g wet wt. for kidneys, and 0.04 μg/g wet wt. (n = 1) for brain. C_{60} concentrations (mean ± SD) in tissues of the Day 28 rat group were 133 ± 47.5 μg/g wet wt. for lungs, 70.6 ± 32.0 μg/g wet wt. for spleen, 14.8 ± 3.00 μg/g wet wt. for liver, and 0.16 ± 0.04 μg/g wet wt. for kidneys.

Table 1
Concentrations of C_{60} in five tissues and blood of Wistar rats.

Group	Sample no.	Concentrations (μg/g wet wt.)					
		Lungs	Spleen	Liver	Kidneys	Brain	Blood
Day 1	1	223	46.5	19.9	1.10	0.080	<0.020
	2	207	78.6	20.8	0.807	0.074	<0.020
	3	188	34.8	32.4	1.14	0.062	<0.020
	4	456	38.7	30.2	0.954	0.078	<0.020
	5	197	66.4	24.5	2.49	0.096	<0.020
Day 7	6	152	52.1	23.0	0.542	0.029	<0.020
	7	281	56.8	18.8	0.508	0.034	<0.020
	8	235	45.0	39.1	0.431	0.048	<0.020
	9	259	28.7	15.4	0.292	0.032	<0.020
	10	66.9	43.8	16.9	0.327	0.037	<0.020
Day 14	11	105	68.3	17.8	0.200	<0.023	<0.020
	12	74.0	51.0	27.9	0.235	<0.023	<0.020
	13	67.5	62.1	17.9	0.200	0.035	<0.020
	14	103	75.1	19.3	0.168	<0.023	<0.020
	15	196	38.8	26.7	0.189	<0.023	<0.020
Day 28	16	113	110	11.4	0.129	<0.023	<0.020
	17	204	94.9	16.6	0.111	<0.023	<0.020
	18	142	68.2	18.3	0.156	<0.023	<0.020
	19	133	44.4	12.0	0.191	<0.023	<0.020
	20	74.1	35.1	15.8	0.191	<0.023	<0.020

4. Discussion

4.1. Biodistribution of C_{60} in rats

C_{60} concentrations in tissues and blood of rats after tail vein injection are investigated (Table 1). C_{60} was detected in the lungs, spleen, liver, and kidneys of rats in all groups, ranging from 0.16 ± 0.04 μg/g wet wt. (kidneys, Day 28) to 254 ± 114 μg/g wet wt. (lungs, Day 1). The highest C_{60} concentration was detected in the lungs, followed by spleen, liver, and kidneys. On the other hand, although C_{60} was detected in all of the brains from the Day 1 and Day 7 groups (0.08 ± 0.01 μg/g wet wt. for Day 1; 0.04 ± 0.01 μg/g wet wt. for Day 7), C_{60} was detected in only one brain specimen from the Day14 group (0.04 μg/g wet wt.) and none of the specimens from the Day 28 group. Moreover, no C_{60} was observed in blood samples from any of the groups. Although studies of the biodistribution of unmodified C_{60} are limited, several studies have reported the biodistribution of water-soluble C_{60} derivatives. Yamago et al. (1995) reported the biodistribution of ^{14}C-labeled water-soluble C_{60} in Fischer rats after intravenous injection. After injection, ^{14}C-labeled water-soluble C_{60} was rapidly removed from blood and about 80% of ^{14}C-labeled water-soluble C_{60} was retained

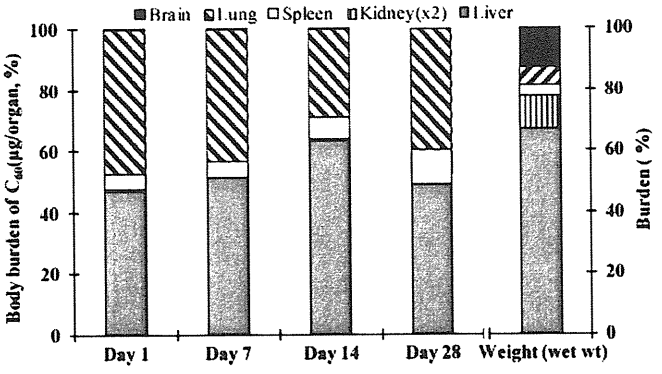

Fig. 3. Comparison of C_{60} distribution in tissues of the four treated rat groups (Days 1, 7, 14, and 28).

in the liver until after 30 h. Furthermore, ^{14}C-labeled water-soluble C_{60} was also detected as a minor component in the spleen, lungs, kidneys, heart, testicles, and brain (Yamago et al., 1995). Bullard-Dillard et al. (1996) reported that a ^{14}C-labeled C_{60} where the label is part of the C_{60} cage after injection in Sprague–Dawley rats was rapidly cleared from the circulation with the majority of the radiolabel accumulated in the liver (90–95%) and ^{14}C-labeled C_{60} was not eliminated from the liver over the 120 h. Moreover, ^{14}C-labeled water-soluble C_{60} derivative was found in liver (>50%) with another 28% distributed between muscle, skin, and lung (Bullard-Dillard et al., 1996). Nikolić et al. (2009) indicated that significantly higher accumulation of radiolabeled C_{60} (^{125}I-nanoC_{60}) was observed in liver as well as spleen, while the accumulation of radiolabeled C_{60} was lower in the lungs, intestines and bone of Wistar rats after intravenous injection. Furthermore, Cagle et al. (1999) showed the selective localization of water-soluble radioactive metallofullerene in the liver of BALB/c mice after intravenous administration. In contrast, although C_{60} was found in the lungs, spleen, liver, kidneys, and brain, in our study the highest concentration of C_{60} was observed in the lungs and the trend differed from the other studies (Yamago et al., 1995; Bullard-Dillard et al., 1996; Cagle et al., 1999; Nikolić et al., 2009). In this study, C_{60}-liposome was suspended in the administration solution, and the C_{60} was an unmodified form. Hence, the difference in the biodistribution of C_{60} between previous studies and this study might be attributable to differences in physical properties, the particle size distribution of C_{60} in the administration solution, and/or period after completion of the injections. Compared with previous studies, the C_{60} particle size in the administration solution for this study seems large (particle size: >100 nm, particle size was obtained from measuring of diluted administration solution by Zetasizer Nano, Malvern Instruments Ltd.) because the C_{60} water solubility is low. We considered that C_{60} injected in the tail vein could be filtered by lung capillary vessels and accumulate in the lungs prior to being distributed to other tissues. C_{60} not being detected in the blood indicates that clearance of C_{60} from the blood by filtration might effectively occur in the lungs. Although C_{60} concentrations were low (0.029–0.096 μg/g wet wt.), C_{60} was detected in the brain. Yamago et al. (1995) and Cagle et al. (1999) have also reported that C_{60} was observed in the brain at low concentrations. These results suggest that a low concentration of C_{60} can pass through the blood brain barrier and accumulate in the brain.

The distribution of C_{60} burden among the five rat tissues was calculated from the product of the C_{60} concentration in each tissue and the weight of each tissue (Fig. 3). Among five tissues, the C_{60} burden was highest in the liver (47.3–63.6%), followed by the lungs (29.0–47.5%), spleen (4.9–11.1%), kidneys (0.1–0.4%), and brain (0–0.03%). Although C_{60} concentrations in the liver were lower than those in the lungs and spleen, the liver showed a higher percentage of C_{60} burden (47.3–63.6%) as a result of the large liver mass (67.0%). On the other hand, although the spleen and lungs accounted for 3.2% and 6.2% of the mass of the five tissues, respectively, the C_{60} burdens were 4.9–11.1% for the spleen and 29.0–47.5% for the lungs, respectively. These three tissues accounted for approximately 100% of the C_{60} burden, indicating that C_{60} was localized to the lungs, spleen, and liver. Because capillary vessels are abundant in these tissues, C_{60} might accumulate by filtration in these tissues. In this study, we focused on the lungs, spleen, liver, kidneys, and brain as major target organs, and other tissues, urine and feces of each specimen were not collected. Although several studies reported the detection of C_{60} derivatives in other tissues (such as, bone, fat, heart, intestines, muscle, and testicles), C_{60} derivatives in these tissues were mostly observed as minor components (Yamago et al., 1995; Bullard-Dillard et al., 1996; Cagle et al., 1999; Nikolić et al., 2009). Further studies should evaluate the metabolic and excretion pathways of C_{60} in experimental animals to understand the toxicokinetics of C_{60}.

4.2. Time-dependent variation in the biodistribution of C_{60} in rats

The time-dependent variation in the biodistribution of C_{60} in rats was examined by comparison of C_{60} concentrations in the five tissues from the four rat groups (Days 1, 7, 14, and 28) (Fig. 4). Although the number of samples for each group was small ($n = 5$), a time-dependent decrease in C_{60} concentrations was observed in all tissues, except the spleen. A significant decrease in C_{60} concentration was found in the kidneys and brain. In the case of the kidneys, significant difference in C_{60} concentration from the four treated groups was found (Kruskal–Wallis test, $p = 0.0007$). C_{60} concentrations from the Day 14 group were significantly lower than those from the Day 1 group (Scheffe's test, $p = 0.0396$). Moreover, C_{60} concentrations from the Day 28 group were also significantly lower than those of the Day 1 group (Scheffe's test, $p = 0.0024$). In the case of the brain, C_{60} concentrations from the Day 7 group were significantly lower than those from the Day 1 group (Student's t-test, $p = 0.0002$). Furthermore, C_{60} concentrations of the Day 14 and Day 28 groups were also lower than those of the Day 7 group. On the other hand, in the lungs and liver, the decreasing trend in C_{60} concentration was slower as compared with the trend in the kidneys and brain. In the case of the lungs, significant difference in C_{60} concentration from the four treated groups was found (Kruskal–Wallis test, $p = 0.0493$) and C_{60} concentrations from the Day 14 group were significantly lower than those from the Day 1 group (Mann–Whitney's U-test, $p = 0.0163$). In the case of the liver, significant difference in C_{60} concentration from the four treated groups was found (Kruskal–Wallis test, $p = 0.0251$) and C_{60} concentrations from the Day 28 group were significantly lower than those from the Day 1 group (Scheffe's test, $p = 0.0298$).

Although with shorter experimental periods than this study, several studies have reported a time-dependent variation in the concentration of C_{60} derivatives in tissues. Yamago et al. (1995) reported the time-dependent change in tissue radioactivity levels using ^{14}C-labeled water-soluble C_{60}. In the liver, about 80% of the total radioactivity was retained after 30 h, and was mostly eliminated (1.6%) after 160 h. This decrease in radioactivity was also observed in the spleen, lungs, and brain. Cagle et al. (1999) also reported the time-dependent decrease of water-soluble radioactive metallofullerene in liver, kidneys, lungs, spleen, and brain after 48 h. Although these studies found a time-dependent decrease of C_{60} derivatives in various tissues, differences in the decreasing trend of the C_{60} derivatives among tissues were not observed. In our study, different decreasing trends of C_{60} among tissues were observed. In the kidneys and brain, a significant decrease in C_{60} concentration was observed. On the other hand, C_{60} concentration

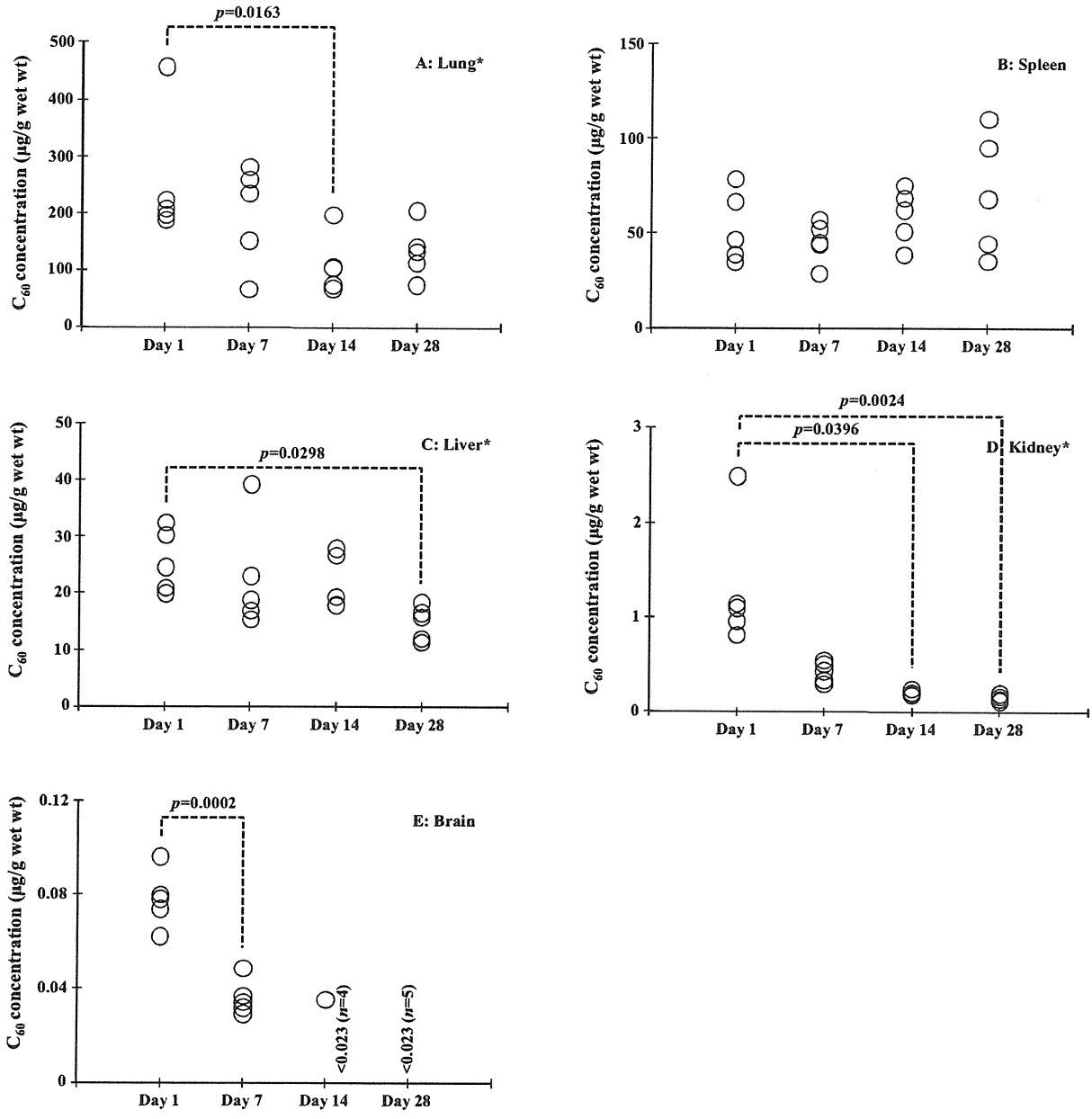

Fig. 4. Comparison of C_{60} concentrations in each tissue of the four treated rat groups (Days 1, 7, 14, and 28). Kruskal–Wallis test was used for validation of difference in the C_{60} concentrations in four tissues among treated groups and significant difference (*) was observed in lungs ($p = 0.0493$), liver ($p = 0.0251$), and kidneys ($p = 0.0007$). (A) C_{60} concentration in lungs (Day 14 vs. Day 1, $p = 0.0163$ (Mann–Whitney's U-test)). (B) C_{60} concentration in spleen. (C) C_{60} concentration in liver (Day 28 vs. Day 1, $p = 0.0298$ (Scheffe's test)). (D) C_{60} concentration in kidneys (Day 14 vs. Day 1, $p = 0.0396$ (Scheffe's test); Day 28 vs. Day 1, $p = 0.0024$ (Scheffe's test)). (E) C_{60} concentration in brain (Day 7 vs. Day 1, $p = 0.0002$ (Student's t-test)).

in lungs and liver decreased gradually. This difference of decreasing trends among tissues could be due to differences in accumulation levels. The low concentration of C_{60} in the kidneys and brain might be easily decreased compared to the high concentrations of C_{60} in the lungs, liver, and spleen. Although it is not clear whether C_{60} is excreted from the body, we propose some possible mechanisms for the decrease of C_{60} in tissues. The first possible mechanism is redistribution to other tissues via blood. Although only five tissues were examined in this study, C_{60} might be detectable in other organs. Cagle et al. (1999) reported a comparatively high concentration of water-soluble radioactive metallofullerene in bone. Moreover, although the accumulation levels were low, radiolabeled nano C_{60} (^{125}I-nanoC_{60}) was found in intestines and bone of rats (Nikolić et al., 2009). Although the C_{60} concentration in blood was below the limit of detection, the small blood volume used for the analysis could be the reason for this result. If a larger volume of blood were analyzed, C_{60} might be detected. Bullard-Dillard et al. (1996) reported that 0.39% of ^{14}C-labeled C_{60} was detected in blood of rat at 120 h post-injection. The second possible mechanism is metabolism to water-soluble fullerene metabolites and excretion into urine. Although there is no information on the intravital metabolism of C_{60}, it is possible that C_{60} could be metabolized to C_{60} derivatives (e.g. fullerenol ($C_{60}(OH)_n$)) by metabolic enzymes (e.g. cytochrome P450). Hamano et al. (1995) identified the structures of $C_{60}O$, $C_{60}O_2$, and $C_{60}O_3$ formed in P450 chemical model systems and the results support the hypothesis that possibility of a biotransformation of C_{60} into more hydrophilic C_{60} derivative capable of being excreted into the urine. In this study, the renal C_{60} concentration rapidly decreased, which also supports the possibility that C_{60} is excreted from urine. The third possible mechanism is biliary

excretion of unmodified C_{60} and/or C_{60} metabolites. Because C_{60} is lipophilic, if C_{60} is excreted without metabolism, it might be via this route. Consequently, further studies are required to verify the metabolism and excretion of C_{60}. Yamago et al. (1995) reported that virtually all of the excretion of ^{14}C-labeled water-soluble C_{60} occurred via the feces and 5.4% of ^{14}C-labeled water-soluble C_{60} was eliminated into the feces after 160 h in intravenous injection experiment. Moreover, Cagle et al. (1999) also indicated that a water-soluble radioactive metallofullerene was excreted into the feces of rats.

In summary, the current study demonstrates that C_{60} after tail vein administration is widely distributed between various tissues, such as brain, kidneys, liver, lungs, and spleen of rats. Moreover, the large variability in C_{60} concentrations among tissues was found and the highest C_{60} concentration was observed in the lungs, followed by spleen, liver, kidneys, and brain. These results suggested that C_{60} injected in the tail vein could be filtered by lung capillary vessels and accumulate in the lungs prior to being distributed to other tissues. Furthermore, C_{60} not being detected in the blood indicates that clearance of C_{60} from the blood by filtration might effectively occur in the lungs. A time-dependent decrease in C_{60} concentrations was observed in all tissues, except spleen. Moreover, a decreasing trend of C_{60} levels differed among tissues, which could be due to differences in accumulation. These results suggest that unmodified C_{60} and/or C_{60} metabolites by metabolic enzymes could be excreted into feces and/or urine. In further studies, the metabolic and excretion pathways of C_{60} should be evaluated to understand the toxicokinetics of C_{60}.

Conflict of interest

The authors declare that there are no conflicts of interest.

Acknowledgement

We are grateful to Miss Rika Maekawa and Mr. Masaki Tsuji for technical support. This study was supported by H21-kagaku-ippan-008 from the Ministry of Health, Labour and Welfare, Japan.

References

Bosi, S., Da Ros, T., Spalluto, G., Prato, M., 2003. Fullerene derivatives: an attractive tool for biological applications. Eur. J. Med. Chem. 38 (11–12), 913–923.
Bullard-Dillard, R., Creek, K.E., Scrivens, W.A., Tour, J.M., 1996. Tissue sites of uptake of ^{14}C labeled C_{60}. Bioorg. Chem. 24 (4), 376–385.
Cagle, D.W., Kennel, S.J., Mirzadeh, S., Alford, J.M., Wilson, L.J., 1999. In vivo studies of fullerene-based materials using endohedral metallofullerene radiotracers. Proc. Natl. Acad. Sci. U.S.A. 96, 5182–5187.
Colvin, V.L., 2003. The potential environmental impact of engineered nanomaterials. Nat. Biotechnol. 21 (10), 1166–1170.
Dugan, L.L., Turetsky, D.M., Du, C., Lobner, D., Wheeler, M., Almli, C.R., Shen, C.K.F., Luh, T.Y., Choi, D.W., Lin, T.S., 1997. Carboxyfullerenes as neuroprotective agents. Proc. Natl. Acad. Sci. U.S.A. 94, 9434–9439.
Friedman, S.H., DeCamp, D.L., Sijbesma, R.P., Srdanov, G., Wudl, F., Kenyon, G.L., 1993. Inhibition of the HIV-1 protease by fullerene derivatives: model building studies and experimental verification. J. Am. Chem. Soc. 115, 6506–6509.
Hamano, T., Mashino, T., Hirobe, M., 1995. Oxidation of [60]fullerene by cytochrome P450 chemical models. J. Chem. Soc. Chem. Commun. 15, 1537–1538.
Kroto, H.W., Heath, J.R., O'Brien, S.C., Curl, R.F., Samlley, R.E., 1985. Nature 318 (14), 162–163.
Kubota, R., Tahara, M., Shimizu, K., Sugimoto, N., Hirose, A., Nishimura, T., 2009. Development of a liquid chromatography–tandem mass spectrometry method for the determination of fullerenes C_{60} and C70 in biological samples. Bull. Natl. Inst. Health Sci. 127, 65–68.
Moore, M.N., 2006. Do nanoparticles present ecotoxicological risks for the health of the aquatic environment? Environ. Int. 32, 967–976.
Moussa, F., Pressac, M., Genin, E., Roux, S., Trivin, F., Rassat, A., Célin, R., Szwarc, H., 1997. Quantitative analysis of C_{60} fullerene in blood and tissues by high-performance liquid chromatography with photodiode-array and mass spectrometric detection. J. Chromatogr. B 696, 153–159.
Nakamura, E., Isobe, H., 2003. Functionalized fullerenes in water. 2003. The first 10 years of their chemistry, biology, and nanoscience. Acc. Chem. Res. 36 (11), 807–815.
Nikolić, N., Vranjes-Ethurić, S., Janković, D., Ethokić, D., Mirković, M., Bibić, N., Trajković, V., 2009. Preparation and biodistribution of radiolabeled fullerene C_{60} nanocrystals. Nanotechnology 20, 385102.
Nel, A., Xia, T., Mädler, L., Li, N., 2006. Toxic potential of materials at the nanolevel. Science 3, 622–627.
Sayes, C.M., Gobin, A.M., Ausman, K.D., Mendez, J., West, J.L., Colvin, V.L., 2005. Nano-C_{60} cytotoxicity is due to lipid peroxidation. Biomaterials 26, 7587–7595.
Tokuyama, H., Yamago, S., Nakamura, E., 1993. Photoinduced biochemical activity of fullerene carboxylic acid. J. Am. Chem. Soc. 115, 7918–7919.
Xia, X.R., Monteiro-Riviere, N.A., Riviere, J.E., 2006. Trace analysis of fullerenes in biological samples by simplified liquid–liquid extraction and high-performance liquid chromatography. J. Chromatogr. A 1129, 216–222.
Yamago, S., Tokuyama, H., Nakamura, E., Kikuchi, K., Kananishi, S., Sueki, K., Nakahara, H., Enomoto, S., Ambe, F., 1995. In vivo biological behavior of a water-miscible fullerene: ^{14}C labeling, absorption, distribution, excretion and acute toxicity. Chem. Biol. 2, 385–389.